Surface electronic structure of K- and Cs-induced √21×√21 phases on Ag/Si(111)√3×√3

Hanmin Zhang, Kazuyuki Sakamoto and Roger I.G. Uhrberg

Original Publication:

Hanmin Zhang, Kazuyuki Sakamoto and Roger I.G. Uhrberg, Surface electronic structure of K- and Cs-induced √21×√21 phases on Ag/Si(111)√3×√3, 2004, Physical Review B. Condensed Matter and Materials Physics, (70), 24, 245301.
http://dx.doi.org/10.1103/PhysRevB.70.245301

Surface electronic structure of K- and Cs-induced $\sqrt{21}\times\sqrt{21}$ phases on Ag/Si(111)$\sqrt{3}\times\sqrt{3}$

H. M. Zhang*
Department of Physics and Measurement Technology, Linköping University, S-581 83 Linköping, Sweden

Kazuyuki Sakamoto
Department of Physics, Graduate School of Science, Tohoku University, Sendai 980-8578, Japan

R. I. G. Uhrberg
Department of Physics and Measurement Technology, Linköping University, S-581 83 Linköping, Sweden
(Received 30 March 2004; revised manuscript received 5 August 2004; published 1 December 2004)

A $\sqrt{21}\times\sqrt{21}$ reconstruction has been formed by adding either K or Cs atoms on the Ag/Si(111)$\sqrt{3}\times\sqrt{3}$ surface at 120 K. The electronic structures of these surfaces have been studied by angle-resolved valence band and core-level spectroscopy. In similarity with Ag or Au adatoms, the presence of K or Cs adatoms on Ag/Si(111)$\sqrt{3}\times\sqrt{3}$ results in a metallic $\sqrt{21}\times\sqrt{21}$ surface. The formation of two surface bands near the Fermi level can be explained by band folding of a partially occupied surface band originating from the underlying Ag/Si(111)$\sqrt{3}\times\sqrt{3}$ surface. A detailed analysis of the Si 2*p* core-level spectra of the above surfaces is presented and compared to the Ag/Si(111)$\sqrt{3}\times\sqrt{3}$ surface. In the case of Ag/Si(111)$\sqrt{3}\times\sqrt{3}$, we find that the metallic tail of the Si 2*p* spectra is related to extra Ag. Both the valence band and the Si 2*p* spectra of the Ag/Si(111)$\sqrt{3}\times\sqrt{3}$ surface show that the surface is semiconducting after annealing at ~600°C.

DOI: 10.1103/PhysRevB.70.245301 PACS number(s): 73.20.−r, 68.35.−p, 79.60.−i

I. INTRODUCTION

During the last decades the Ag/Si(111)$\sqrt{3}\times\sqrt{3}$ surface has been the focus of many studies as a prototypical metal/semiconductor interface. A special property of this surface is that it acts as a substrate on which superstructures can be formed by additional noble metal adatoms (Ag, Au, Cu). An interesting observation is the coverage-dependent semiconductor/metal transition caused by extra Ag adatoms on the $\sqrt{3}\times\sqrt{3}$ surface. The presence of the extra Ag adatoms, with one loosely bound *s* electron each, leads to a partial filling of an unoccupied surface state band (S_1) of the underlying $\sqrt{3}\times\sqrt{3}$ substrate. This results in a metallic $\sqrt{21}\times\sqrt{21}$ surface. Further evaporation of Ag atoms changes the $\sqrt{21}\times\sqrt{21}$ phase into a semiconducting 6×6 phase.[1,2] The above observations have motivated us to perform a detailed study of the surface electronic structure for the K- and Cs-induced reconstructions on Ag/Si(111)$\sqrt{3}\times\sqrt{3}$, since K and Cs also have an outer loosely bound *s* electron.

The Ag/Si(111)$\sqrt{3}\times\sqrt{3}$ surface is formed by annealing a Si(111)7×7 surface covered by one monolayer (ML) of Ag atoms. Recently, there are some developments regarding its atomic and electronic structure. An inequivalent triangle (IET) model[3] was suggested for the ground state of the Ag/Si(111)$\sqrt{3}\times\sqrt{3}$ phase instead of the honeycomb-chain-trimer (HCT) model which has been widely used in the literature.[4] A difference between the two models is that there are two types of Ag trimers with different sizes in the IET model, while there is only one type of Ag trimer in the HCT model. Another finding is the effect of additional Ag atoms that is often neglected in many surface studies.[5] When the additional Ag atoms are removed from the surface, the valence band spectra of the Ag/Si(111)$\sqrt{3}\times\sqrt{3}$ surface show an intrinsically semiconducting character.[6] Obviously, the additional Ag atoms play an important role for the surface electronic properties of the Ag/Si(111)$\sqrt{3}\times\sqrt{3}$ surface. The change in the surface electronic structure with increasing Ag density is also accompanied by a change of the atomic periodicity. A $\sqrt{21}\times\sqrt{21}$ phase appears below 250 K with an additional ~0.15 ML of Ag, and a 6×6 phase that is stable only at low temperature (LT, 100 K) is obtained at an additional ~0.22 ML of Ag.[2,7] In similarity with the noble metals (Ag, Au, Cu), alkali metals (K, Cs) also form superstructures on the Ag/Si(111)$\sqrt{3}\times\sqrt{3}$ surface. Three reconstructions have been found when adding K atoms on Ag/Si(111)$\sqrt{3}\times\sqrt{3}$ at room temperature (RT), i.e., a $\sqrt{21}\times\sqrt{21}$, a 6×6, and a $2\sqrt{3}\times2\sqrt{3}$ phase.[8] In the case of Cs, a $\sqrt{21}\times\sqrt{21}$ and a 6×6 phase have been observed at RT. An interesting property of the various $\sqrt{21}\times\sqrt{21}$-(Ag, Au, Cu, K, Cs) phases is that they all show an anomalously high surface conductance compared to the initial $\sqrt{3}\times\sqrt{3}$ surface.[8] The high surface conductance has been explained in terms of two metallic bands on the Au-induced $\sqrt{21}\times\sqrt{21}$ surface.[9] However, a detailed investigation of our photoemission data shows that there is only one metallic band on the $\sqrt{21}\times\sqrt{21}$ surface. The low conductance of both the $\sqrt{3}\times\sqrt{3}$ and the 6×6 surface is related to the semiconducting character of their surface electronic structures.[2] From earlier scanning tunneling microscopy (STM) studies of $\sqrt{21}\times\sqrt{21}$-Au, it was reported that the additional Au adatoms are sitting on the Ag trimer sites and the underlying $\sqrt{3}\times\sqrt{3}$ framework still remains.[10,11] Since both $\sqrt{21}\times\sqrt{21}$-K and -Cs show a similar result in surface conductance measurements, it is generally believed that the same conclusions should apply to the K and Cs cases. In a recent photoemission study of the Cs-induced $\sqrt{21}\times\sqrt{21}$ surface,[12] two broad surface state bands were observed near the Fermi level. The appearances of these surface bands are signifi-

cantly different from the $\sqrt{21}\times\sqrt{21}$-Ag and -Au spectra. This, together with STM data, led the authors to conclude that the framework of the underlying $\sqrt{3}\times\sqrt{3}$ substrate is totally broken, and thus the $\sqrt{21}\times\sqrt{21}$-Cs phase is an exceptional case. According to the phase diagram in Ref. 8, it seems that there are two types of $\sqrt{21}\times\sqrt{21}$-Cs phases at different Cs coverage, as observed by reflection high-energy electron diffraction. The $\sqrt{21}\times\sqrt{21}$-Cs phase in Ref. 12 was prepared at room temperature and appeared after a 6×6 phase. It is likely that they obtained the second $\sqrt{21}\times\sqrt{21}$ phase, which is formed at a higher coverage. In any case, we find that our photoemission result does not support the conclusions in Ref. 12.

In this paper, the surface electronic structures of the $\sqrt{21}\times\sqrt{21}$-K and -Cs surfaces have been investigated by angle-resolved photoelectron spectroscopy (ARPES) and core-level spectroscopy. The K and Cs-induced $\sqrt{21}\times\sqrt{21}$ surfaces show six dispersive surface state bands, which are quite similar to the Ag- and Au- induced $\sqrt{21}\times\sqrt{21}$ surfaces. The presence of K or Cs adatoms results in a metallic $\sqrt{21}\times\sqrt{21}$ surface with two surface state bands near the Fermi level. These two bands are split at the $\sqrt{21}\times\sqrt{21}$ zone boundary with a gap of about 0.35 eV. The formation of these two bands can be explained by band folding of S_1 into the $\sqrt{21}\times\sqrt{21}$ surface Brillouin zone (SBZ) with an interaction potential $U\sim0.18$ eV.

II. EXPERIMENTAL DETAILS

The photoemission study was performed at beam line 33, at the MAX-lab synchrotron radiation facility in Lund, Sweden. The angle resolved valence band spectra presented here were obtained with a total energy resolution of ~50 meV and an angular resolution of ±2°. The Si 2*p* core-level spectra had an energy resolution of ~90 meV and an angular resolution of ±2°. An *n*-type Si(111) sample was cut from a single crystal wafer with Sb-doping (3 Ω cm) and a *p*-type sample was cut from a B-doped (6 m Ω cm) wafer. The samples were preoxidized by an etching method and cleaned *in situ* by either stepwise direct current heating up to ~940 °C or high temperature flashing at ~1250 °C. Both procedures resulted in a well-ordered surface, as evidenced by the strong surface state emission and a sharp 7×7 low-energy electron diffraction (LEED) pattern. Evaporation of 1 ML of Ag from a tungsten filament source followed by annealing at ~530 °C for 2 min resulted in a sharp $\sqrt{3}\times\sqrt{3}$ LEED pattern. The sample was then annealed at ~600 °C to remove extra Ag monitored by both LEED and valence band photoemission. K and Cs were evaporated onto the LT (120 K) $\sqrt{3}\times\sqrt{3}$ surface from getter sources (SAES Getters) in a preparation chamber. The quality of the $\sqrt{21}\times\sqrt{21}$-K and -Cs surfaces were optimized using both LEED and photoelectron spectroscopy. The $\sqrt{21}\times\sqrt{21}$-K and -Cs LEED patterns [Figs. 1(a) and 1(b)] are as good as the Ag-induced one (Fig. 1 in Ref. 2). Further evaporation of K and Cs at LT (120 K) did not induce any other reconstruction. At RT, in the case of K, a 6×6 [Fig. 1(c)] and a $2\sqrt{3}\times2\sqrt{3}$ [Fig. 1(d)] phase appear after the $\sqrt{21}\times\sqrt{21}$ phase. In the case of Cs, only a $\sqrt{21}\times\sqrt{21}$ and a 6×6 phase were observed at RT. However, we found that the $\sqrt{21}\times\sqrt{21}$-K and -Cs phases were easily affected even by LEED at room temperature.

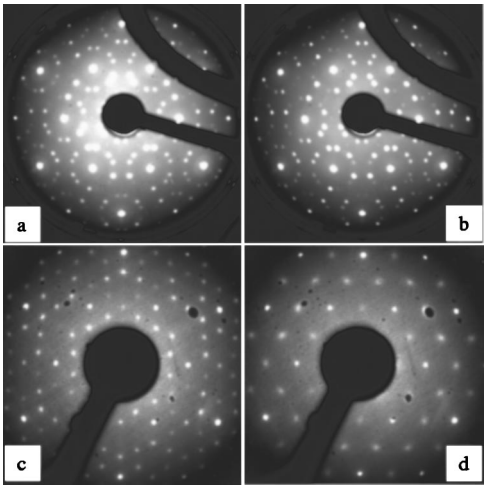

FIG. 1. K- and Cs-induced LEED patterns on Ag/Si(111)$\sqrt{3}\times\sqrt{3}$. (a) $\sqrt{21}\times\sqrt{21}$-K at 100 K, 64 eV. (b) $\sqrt{21}\times\sqrt{21}$-Cs at 100 K, 64 eV. (c) 6×6-K surface at RT, 61 eV; (d) $2\sqrt{3}\times2\sqrt{3}$-K at RT, 63 eV.

III. RESULTS AND DISCUSSION

A. Surface band structures of the $\sqrt{21}\times\sqrt{21}$-K and -Cs surfaces

Angle-resolved photoemission spectra from the $\sqrt{21}\times\sqrt{21}$-K and -Cs surfaces obtained at 100 K along the $\bar{\Gamma}$-$\bar{M}$-$\bar{\Gamma}$ line of the $\sqrt{3}\times\sqrt{3}$ SBZ are shown in Fig. 2. Since the $\sqrt{21}\times\sqrt{21}$ phase can be regarded as a superstructure based on the underlying $\sqrt{3}\times\sqrt{3}$ substrate,[10,11] we use the $\sqrt{3}\times\sqrt{3}$ SBZ to describe the azimuthal directions of the $\sqrt{21}\times\sqrt{21}$ reconstructions. The *n*-type Si(111) sample that was used in this case was cleaned at ~940 °C. Except for a large surface photovoltage (SPV) shift toward higher binding energy, the K- or Cs-induced $\sqrt{21}\times\sqrt{21}$ surface has an electronic structure that is almost identical to the Ag-induced one. Six surface state bands S_1-S_6 were detected in the valence spectra. All are present in Fig. 2, except for S_3, which appears more clearly for smaller emission angles. Two surface states S_1 and S_4 are important for the discussion of the surface conductance measurements of the $\sqrt{21}\times\sqrt{21}$ surfaces. S_4 has a parabolic shape and has been assigned as a metallic band in the case of $\sqrt{21}\times\sqrt{21}$-Ag.[2] The S_1 surface state is located at a minimum energy at $\theta_e=-32°$ and it disperses steeply upward to a maximum energy at $\theta_e=-38°$. S_1 is well-separated from S_4 and it turns downward again beyond $\theta_e=-38°$, as expected from a fully occupied surface state band. Thus, in similarity with the earlier study,[2] our photoemission data show clear resemblances between the different $\sqrt{21}\times\sqrt{21}$ surfaces (Ag, Au, K, and Cs). The formation of S_1 is related to the transfer of *s* electrons from the additional adatoms into the unoccupied surface state band of the $\sqrt{3}\times\sqrt{3}$ surface. From our photoemission studies, we find that the band minimum of S_1 shifts continuously down-

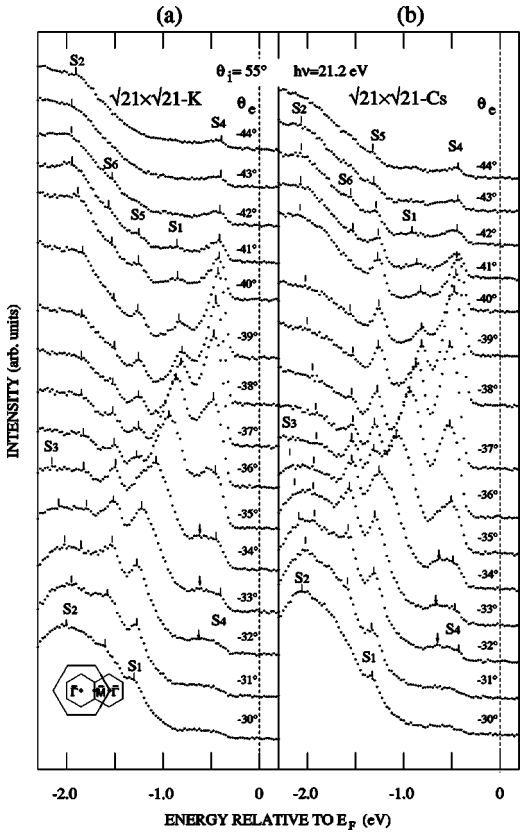

FIG. 2. ARPES spectra recorded with a photon energy of 21.2 eV at 100 K. The *n*-type Si(111) samples were cleaned at 940°C. The emission angles correspond to $\mathbf{k}_{\|}$ points throughout the first and second $\sqrt{3}\times\sqrt{3}$ SBZ, along the $\bar{\Gamma}$-$\bar{M}$-$\bar{\Gamma}$ line (see inset). (a) $\sqrt{21}\times\sqrt{21}$-K; (b) $\sqrt{21}\times\sqrt{21}$-Cs. Six surface state bands are indicated by the labels S_1-S_6. These surfaces show SPV shifts which do not change by shining visible light.

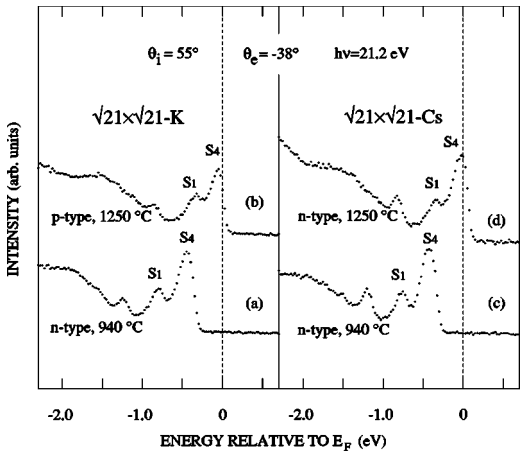

FIG. 3. ARPES spectra recorded with a photon energy of 2.12 eV at an emission angle of −38° at 100 K. The left panel shows $\sqrt{21}\times\sqrt{21}$-K and the right panel shows $\sqrt{21}\times\sqrt{21}$ -Cs under the different sample conditions. (a) 940°C annealed *n*-type sample; the surface shows a constant SPVshift of ~0.35 eV with or without visible light. (b) 1250°C annealed *p*-type sample; the surface does not show a SPV shift. (c) 940°C *n*-type sample; the surface shows a constant SPV shift of ~0.35 eV with or without visible light. (d) 1250°C annealed *n*-type sample, with visible light; the surface shows an opposite SPV shift compared to (a) and (c).

ward when more and more adatoms (Ag, Au, K, and Cs) are deposited on the $\sqrt{3}\times\sqrt{3}$ surface. In two-dimensional **k** space, this means that the Fermi circle becomes larger, i.e., the Fermi vector k_F increases. At a certain adatom density, the $\sqrt{21}\times\sqrt{21}$ periodicity will form and a new surface state band (S_4) appears due to band folding of S_1 into the $\sqrt{21}\times\sqrt{21}$ SBZ. In Fig. 2, this is clearly evidenced by a band gap of 0.35 eV between S_4 and S_1 at the $\sqrt{21}\times\sqrt{21}$ SBZ boundary ($\theta_e=-38°$). In fact, a similar gap (Fig. 1 in Ref. 13) has also been observed from the Fermi surface mapping of the $\sqrt{21}\times\sqrt{21}$-Au surface. Comparing the various $\sqrt{21}\times\sqrt{21}$ surfaces, one finds that the gaps between S_4 and S_1 are different. The $\sqrt{21}\times\sqrt{21}$-Ag phase has a gap of ~0.23 eV, while the $\sqrt{21}\times\sqrt{21}$-Au phase has a gap of ~0.20 eV. According to Ref. 13, by using $U=E_g/2$ one can also estimate the interaction potentials for these surfaces. The $\sqrt{21}\times\sqrt{21}$-Ag and -Au phases have small values of 0.12 and 0.10 eV, and a large value of 0.18 eV is obtained for the K- and Cs-induced phases. The difference in interaction potentials between Au, Ag, and K, Cs may simply be related to their ionization energies. Compared to Au and Ag, K and Cs more easily donate their *s* electrons.

Figures 3(a)–3(d) show spectra from the $\sqrt{21}\times\sqrt{21}$-K and -Cs surfaces at $\theta_e=-38°$. Except for some differences in the intensities of S_4 and S_1, these spectra represent $\sqrt{21}\times\sqrt{21}$ surfaces of similar quality. For the *n*-type, ~940°C cleaned samples, both Cs- and K-induced $\sqrt{21}\times\sqrt{21}$ surfaces show significant negative SPV shifts of ~0.35 eV with synchrotron radiation as the only light source (the windows of the ARPES chamber were covered and the ion gauge was off). We found that the SPV shifts did not change when shining visible light onto the samples. This means that the SPV shifts were already saturated by the synchrotron light. To be able to correct the energy scale for the SPV shifts, we have investigated the $\sqrt{21}\times\sqrt{21}$ spectra under various sample conditions. The *p*-type sample used in this study did not show any SPV shift at low temperature (100 K) under the different light conditions. In Fig. 3(b), a $\sqrt{21}\times\sqrt{21}$-K surface prepared on the *p*-type sample shows a metallic surface state with a clear Fermi cut. Compared to the *n*-type sample, the S_4 surface state of the $\sqrt{21}\times\sqrt{21}$-K surface on the *p*-type sample has less intensity and angular dispersion. It is worth noting that the cutoff due to the Fermi-Dirac function will cause a less steep appearance of the S_4 dispersion. The metallic character of $\sqrt{21}\times\sqrt{21}$-K is consistent with $\sqrt{21}\times\sqrt{21}$-Ag. For the *n*-type samples that were cleaned at ~1250°C, the spectra of the $\sqrt{21}\times\sqrt{21}$-K and -Cs surfaces are of similar quality with two well separated surface state bands (S_1 and S_4). Figure 3(d) shows one of these spectra from the $\sqrt{21}\times\sqrt{21}$-Cs surface. Here the Fermi level cuts the S_4 peak at a rather high position. This is due to a positive SPV shift caused by a *p*-type layer near the surface formed during the high temperature ~1250°C annealing.[14]

Figure 4 shows the band dispersions of the K- and Cs-induced $\sqrt{21}\times\sqrt{21}$ surfaces obtained from Fig. 2. Com-

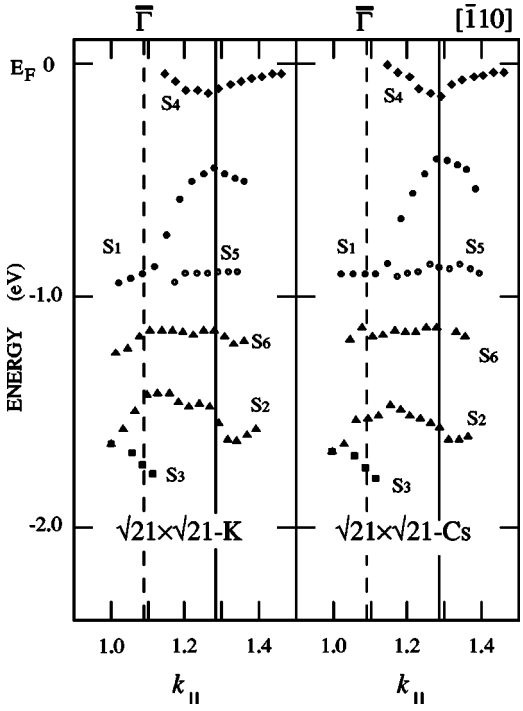

FIG. 4. Dispersions of the surface state bands along the $\bar{\Gamma}$-$\bar{M}$-$\bar{\Gamma}$ line of the $\sqrt{3}\times\sqrt{3}$ SBZ from Fig. 2. (a) $\sqrt{21}\times\sqrt{21}$-K. (b) $\sqrt{21}\times\sqrt{21}$-Cs. The dashed lines indicate the second $\bar{\Gamma}$ point of the $\sqrt{3}\times\sqrt{3}$ SBZ. The solid lines indicate the $\sqrt{21}\times\sqrt{21}$ SBZ boundary.

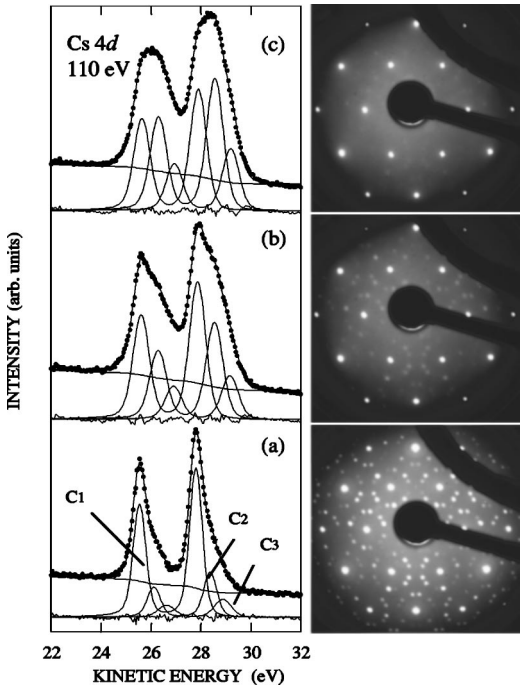

FIG. 5. Cs 4*d* core-level spectra recorded with a photon energy of 110 eV at normal emission and corresponding LEED patterns (96 eV) at 100 K. (a) Cs was evaporated for 6 min. (b) Cs was evaporated for 12 min. (c) Cs was evaporated for 18 min. A spin-orbit splitting of 2.26 eV, a branching ratio of ~0.7, and a singularity index of 0.02 were used in the fitting program. The two small components, C2 and C3, are shifted by 0.6 and 1.1 eV with respect to C1.

pared to the $\sqrt{3}\times\sqrt{3}$ surface [Fig. 3(a) in Ref. 2], the surface band structures of the $\sqrt{21}\times\sqrt{21}$-K and -Cs phases are somewhat complicated. On the other hand, the resemblances between different $\sqrt{21}\times\sqrt{21}$-(Ag,Au,K,Cs) surfaces are very striking. This fact gives a natural explanation why all the $\sqrt{21}\times\sqrt{21}$ phases show a high surface conductance. In similarity with the $\sqrt{21}\times\sqrt{21}$-(Ag,Au) phases, S_5 and S_6 are also clearly observed on $\sqrt{21}\times\sqrt{21}$-K and -Cs. The downward displacements of the S_2 and S_3 surface bands are evident when comparing these bands to the initial $\sqrt{3}\times\sqrt{3}$ surface [Fig. 3(a) in Ref. 2]. The S_5 and S_6 surface bands appear at energies similar to S_2 and S_3 of the Ag/Si(111)$\sqrt{3}\times\sqrt{3}$ surface. This indicates that the surface states of Ag/Si(111)$\sqrt{3}\times\sqrt{3}$ split into two groups due to a partial occupation of the Ag trimer sites by K or Cs atoms. Thus the S_5 and S_6 states have probably the same origin as the initial S_2 and S_3 surface states of the Ag/Si(111)$\sqrt{3}\times\sqrt{3}$ surface.

Obviously, our photoemission result is not consistent with the recent study which reported that the $\sqrt{21}\times\sqrt{21}$-Cs phase is totally different from the Ag- or Au-induced one.[12] Experimentally, it is difficult to actually separate the $\sqrt{21}\times\sqrt{21}$ phase from the $\sqrt{3}\times\sqrt{3}$ phase since the LEED pattern of $\sqrt{21}\times\sqrt{21}$ also contains the $\sqrt{3}\times$ spots. Consequently, this will result in an uncertainty in phase optimization. We have also studied the 6×6-K and -Cs phases that were only obtained at RT. However, the electronic structures of the 6×6 phases show featureless spectra with two broad surface state bands near the Fermi level, and the bulk-like Si 2*p* core-level spectra show a long tail on the low binding energy side. These results are very different from the 6×6-Ag phase. Figure 5 shows spectra of the Cs 4*d* core-level and LEED patterns for three consecutive evaporations (6 min each) at 120 K. The spectrum in Fig. 5(a) was recorded after the valence band series in Fig. 2(b). Except for a large component (C_1), there exist also two small components (C_2 and C_3) at high kinetic (low binding) energies. An increase in the amount of Cs results in a lower quality of the $\sqrt{21}\times\sqrt{21}$ LEED pattern. After the third evaporation (a total of 18 min), LEED basically shows a strong $\sqrt{3}\times\sqrt{3}$ pattern. In Figs. 5(b) and 5(c) the additional Cs 4*d* intensity grows on the low binding energy side. Thus, C_2 and C_3 may come from Cs atoms on the $\sqrt{3}\times\sqrt{3}$ overlayer which do not belong to the $\sqrt{21}\times\sqrt{21}$ phase. In Fig. 2, there is a small feature below S_4 (marked by an arrow) around an emission angle of −32° in both the K and Cs cases. This feature does not appear in the spectra of the $\sqrt{21}\times\sqrt{21}$-(Ag, Au) surfaces. We tentatively assign it as a contribution due to a slight overdosing as indicated by the Cs 4*d* spectrum in Fig. 5(a).

B. Si 2*p* core-level spectra of the Ag/Si(111)$\sqrt{3}\times\sqrt{3}$ surface

From an earlier study, it was reported that the Ag/Si(111)$\sqrt{3}\times\sqrt{3}$ surface shows an intrinsically semiconducting character.[15,16] Later on, this result was questioned by many surface sensitive measurements, such as STM, core-level spectroscopy, and inverse photoemission.[17–20] Those re-

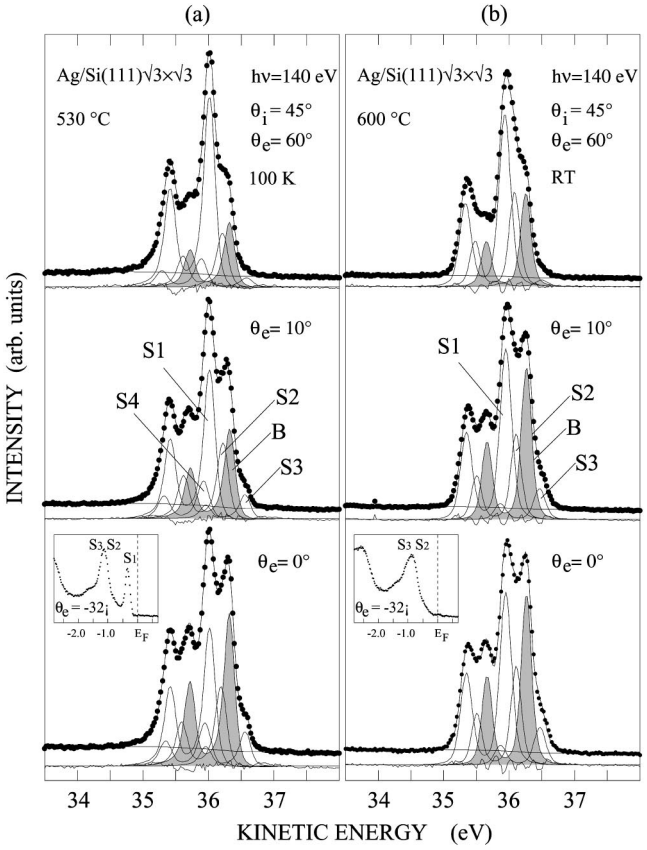

FIG. 6. Si 2*p* core-level spectra recorded with a photon energy of 140 eV at normal emission, 10°, and 60°. (a) $\sqrt{3}\times\sqrt{3}$ after annealing at 530 °C for 2 min, the spectra were recorded at 100 K. The spin-orbit splitting is 0.608 eV. A branching ratio of ~0.55 and a singularity index of 0.02 were used for (a). The S1, S2, S3, and S4 components are shifted by 0.32, 0.12, −0.23, and 0.45 eV with respect to the bulk component. (b) $\sqrt{3}\times\sqrt{3}$ after annealing at 600 °C for 1 min., the spectra were recorded at RT and were fitted without singularity. The S1, S2, and S3 components are shifted by 0.32, 0.14, and −0.20 eV with respect to the bulk component. The valence spectra were recorded with a photon energy of 21.2 eV at an emission angle of −32°, along the $\bar{\Gamma}$-$\bar{M}$-$\bar{\Gamma}$ line of the $\sqrt{3}\times\sqrt{3}$ SBZ.

ports concluded that the Ag/Si(111)$\sqrt{3}\times\sqrt{3}$ surface instead shows a metallic behavior. Here we present our photoemission data and show that the metallic behavior of Ag/Si(111)$\sqrt{3}\times\sqrt{3}$ is related to the extra Ag. Figure 6 shows two sets of high resolution Si 2*p* core-level spectra obtained from the Ag/Si(111)$\sqrt{3}\times\sqrt{3}$ surface at 100 K and at room temperature, respectively. The two sets of spectra were recorded for separate sample preparations. The first surface was annealed at ~530 °C for 2 min after a deposition of 1 ML of Ag. The LT (100 K) spectra in the left panel should be compared with the ones in Ref. 18 and 19. The second surface was further annealed at ~600 °C for 1 min. As shown in the right panel, these spectra are well resolved even at room temperature. LEED showed only sharp $\sqrt{3}\times\sqrt{3}$ patterns with no difference between the two surfaces. The spectra were recorded with a photon energy of 140 eV at normal, 10° and 60° emission angles. Compared to normal emission, the 60° emission spectrum shows an enhancement of the surface component S1. To facilitate a discussion,we also present the corresponding valence band spectra recorded at $\theta_e = -32°$, which is near the second $\bar{\Gamma}$ point along the $\bar{\Gamma}$-$\bar{M}$-$\bar{\Gamma}$ line of the $\sqrt{3}\times\sqrt{3}$ SBZ. The ~530 °C annealed surface shows a strong surface state (S_1), which was assigned as a metallic state in Ref. 16, while a ~600 °C post-annealing removes S_1 and the surface becomes semiconducting. The change in the valence spectra is also reflected in the Si 2*p* core-level spectra. A significant difference is evident in the shape of the low energy tail when comparing the two sets of Si 2*p* spectra. The spectra in the left panel clearly show an extended tail typical for a metallic surface. The metallic line shape was addressed in the recent photoemission studies of the Ag/Si(111)$\sqrt{3}\times\sqrt{3}$ surface.[18,19] In the right panel the spectra obtained after 600 °C annealing show steep edges, indicating a nonmetallic surface. Obviously, the asymmetric tail in the left panel is related to the metallic surface state S_1, which is caused by extra Ag on the $\sqrt{3}\times\sqrt{3}$ surface. When the extra Ag is removed from the surface, as evidenced by the absence of S_1 in Fig. 6(b), the Si 2*p* core-level spectra reveal the semiconducting character.

A fitting procedure has been applied in order to obtain more detailed information. A Voigt line shape with varied Gaussian widths and a fixed Lorentzian full width at half maximum (FWHM) of 80 meV has been used. The Gaussian widths of the bulk components are ~135 and ~140 meV for the LT and RT spectra, respectively. The Gaussian widths of the surface components are ~150 and ~170 meV for the LT and RT spectra, respectively. To fit the spectra in the left panel, we have to use a singularity index of 0.02 in order to take care of the metallic tail, while the spectra in the right panel can be fitted in a satisfactory way without any asymmetry. Another difference between Figs. 6(a) and 6(b) is the number of surface components. It is necessary to use four surface components (S1, S2, S3, and S4) in order to achieve a high quality fit of the spectra in Fig. 6(a). However, in Fig. 6(b) three surface components (S1, S2, and S3) are sufficient to obtain consistent fits throughout the different emission angles. In Fig. 6(b), the intensity of S3 at the highest emission angle is largely reduced. One possible origin of S3 could be domain boundaries that may have a shadowing effect at high emission angles. In a previous study,[6] S1 was assigned to the top Si trimer atoms, S2 to the second layer Si atoms which bond to the Si trimers, and S3 that contains two small features in Ref. 6 was assigned to defects. All these components are clearly present in Fig. 6(b). Thus the core-level spectra in the right panel should be representative of the Ag/Si(111)$\sqrt{3}\times\sqrt{3}$ surface without extra Ag. For the left panel that corresponds to a $\sqrt{3}\times\sqrt{3}$ with extra Ag, the use of S4 is necessary to fit the spectra. The origin of S4 is, however, not entirely understood. One explanation could be that S4 is related to the small amount of extra Ag. Filling of electrons from extra Ag atoms into the unoccupied state (S_1) of $\sqrt{3}\times\sqrt{3}$ leaves positively charged ions on the surface. Consequently, a small amount of the Si atoms, especially those near the positive ions, will shift their core-levels toward higher binding (lower kinetic) energy, resulting in S4.

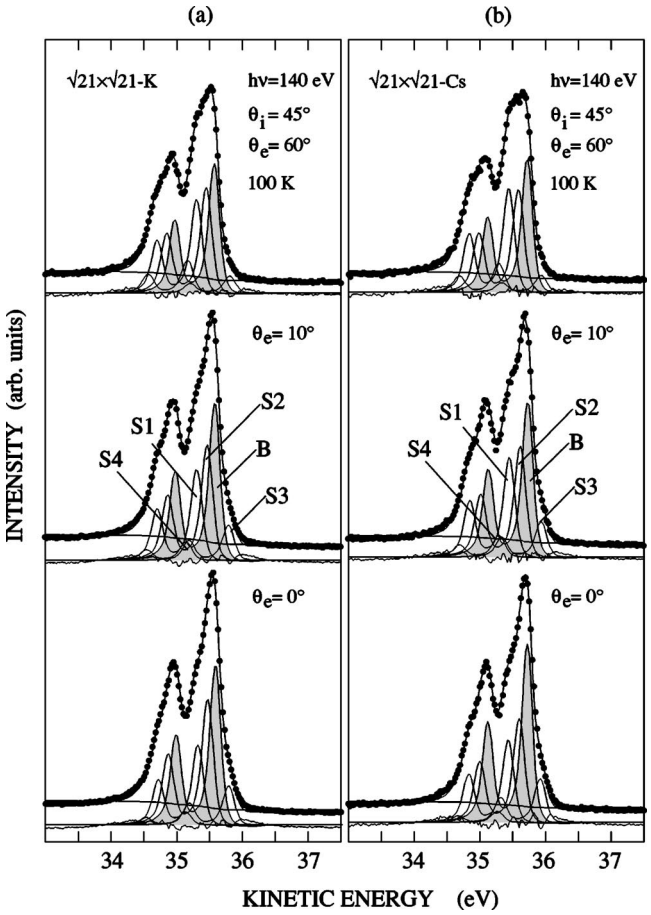

FIG. 7. Si 2*p* core-level spectra recorded with a photon energy of 140 eV at normal emission, 10°, and 60° at 100 K. (a) $\sqrt{21}\times\sqrt{21}$-K. (b) $\sqrt{21}\times\sqrt{21}$-Cs. The spin-orbit splitting is 0.608 eV. A branching ratio of ~0.55, and a singularity of 0.02 were used for all the spectra. The S1, S2, S3, and S4 components are shifted by 0.28, 0.13, −0.20, and 0.44 eV with respect to the bulk component for both the $\sqrt{21}\times\sqrt{21}$-K and -Cs surfaces.

C. Si 2*p* core-level spectra of the $\sqrt{21}\times\sqrt{21}$-K and -Cs surfaces

The Si 2*p* core-level spectra provide another view of the $\sqrt{21}\times\sqrt{21}$ surfaces. Figure 7 shows Si 2*p* core-level spectra for the K and Cs-induced $\sqrt{21}\times\sqrt{21}$ surfaces at 100 K. By comparing the bulk Si 2*p* core-levels from the 7×7 and $\sqrt{3}\times\sqrt{3}$ surfaces at room temperature and using E_F-E_V=0.65 eV as a reference value for 7×7,[21] the Fermi pinning position for Ag/Si(111)$\sqrt{3}\times\sqrt{3}$ is found around 0.1 eV above the valence band maximum (VBM). Due to the SPV effects of the *n*-type samples at low temperature, the energy difference of the bulk Si 2*p* core-level does not directly reflect the change in the Fermi pinning positions between $\sqrt{3}\times\sqrt{3}$ and $\sqrt{21}\times\sqrt{21}$. However, the Si 2*p* bulk component of $\sqrt{21}\times\sqrt{21}$-K from the *p*-type sample, which did not show the SPV effect, is located ~0.4 eV lower in kinetic energy than that of the $\sqrt{3}\times\sqrt{3}$ surface. This value corresponds to an upward shift of the Fermi level for $\sqrt{21}\times\sqrt{21}$ -K compared to the $\sqrt{3}\times\sqrt{3}$ surface. Thus for the $\sqrt{21}\times\sqrt{21}$ surface, the Fermi pinning position is around 0.5 eV above the VBM. For a *n*-type sample with the bulk Fermi position near the conduction band, this means an upward band bending, resulting in a *n*-type SPV shift as observed in Fig. 2.

In a recent photoemission study,[19] the authors presented LT Si 2*p* spectra of the Ag-induced $\sqrt{21}\times\sqrt{21}$ surface. Since their initial $\sqrt{3}\times\sqrt{3}$ spectra show two broad features and the $\sqrt{21}\times\sqrt{21}$-Ag spectrum is also featureless, there is a large uncertainty in the decomposition of the spectra. As illustrated in Fig. 7, the Si 2*p* spectra of both the $\sqrt{21}\times\sqrt{21}$-K and -Cs surfaces show certain features for different emission angles, but they are quite different from the $\sqrt{3}\times\sqrt{3}$ surface (Fig. 6). Evidently, the formation of the $\sqrt{21}\times\sqrt{21}$ periodicity not only changes the valence band structure, but also dramatically affects the Si 2*p* line shape. The $\sqrt{21}\times\sqrt{21}$-K and -Cs surfaces show a metallic character in the valence band spectra as mentioned above. A long tail at the low kinetic energy side of the Si 2*p* core-level spectra in Fig. 7 once again confirms the metallic characters of the $\sqrt{21}\times\sqrt{21}$-K and -Cs surfaces. In fact, all the $\sqrt{21}\times\sqrt{21}$-(Ag, Au, K, Cs) surfaces that we have studied show a striking resemblance from the Si 2*p* core-level spectra. Here, an intriguing task is to find out why the Si 2*p* core-level spectra of the $\sqrt{21}\times\sqrt{21}$ surfaces are so different from those of Ag/Si(111)$\sqrt{3}\times\sqrt{3}$. As illustrated just by the raw spectra in Fig. 7, a dramatic change from $\sqrt{3}\times\sqrt{3}$ to $\sqrt{21}\times\sqrt{21}$ is the reduction of the surface component S1. We have used parameters similar to those in Fig. 6 to fit the $\sqrt{21}\times\sqrt{21}$ spectra. The Gaussian widths of the bulk components are ~140 meV (FWHM) and for the surface components we used ~150 meV for all the spectra. Four surface components are needed to obtain good quality fits of the $\sqrt{21}\times\sqrt{21}$ spectra. The surface component S1 has a shift of 0.28 eV with respect to the bulk component. This value is smaller than the corresponding value of 0.32 eV found in the $\sqrt{3}\times\sqrt{3}$ case. In the 60° emission spectra, the intensity of S1 is reduced by ~50% compared to the $\sqrt{3}\times\sqrt{3}$ surface. The intensities of the S2 and B components, on the other hand, increase by a similar amount.

To properly interpret these changes, we find that it is useful to go back to the valence band picture. On the $\sqrt{3}\times\sqrt{3}$ surface without extra Ag, there exist two surface bands (S_2 and S_3) that are degenerate at the $\bar{\Gamma}$ point of the $\sqrt{3}\times\sqrt{3}$ SBZ. As shown in the valence band spectrum [inset in Fig. 6(b)], S_2 and S_3 are located ~1 eV below the Fermi level near the second $\bar{\Gamma}$ point. When the $\sqrt{21}\times\sqrt{21}$ surface is formed by additional adatoms (Ag, Au, K, Cs), the S_2 and S_3 surface state bands split into two groups and become four bands, denoted S_2, S_3, and S_5, S_6 in Figs. 2 and 4. From STM studies of $\sqrt{21}\times\sqrt{21}$-Au, Nogami *et al.* proposed an atomic model with 5 Au adatoms that sit on Ag trimer sites.[10] The similarity in electronic structure indicates that the same model can also be applied to the $\sqrt{21}\times\sqrt{21}$-K and -Cs phases. Since the K or Cs coverage is only 0.24 ML, the attenuation of the Si 2*p* core-level intensity should be very small, especially if the adatoms are located on Ag trimer sites. Thus, the dramatic change of S1 (Si trimers) might originate from a charge effect, i.e., an uneven redistribution of charges caused by K or Cs atoms. According to STM

studies of the Ag/Si(111)$\sqrt{3}\times\sqrt{3}$ surface,[10,11,22] a Si trimer appears as a black hole in the filled-state images. On a $\sqrt{21}\times\sqrt{21}$ surface there are seven Si trimers per unit cell and they can be grouped into three types as can be seen in Figs. 7 and 8 of Ref. 22. In detail, one is the corner hole in the $\sqrt{21}\times\sqrt{21}$ unit cell surrounded by three bright Ag trimers (Ag trimers with extra Ag on top). There are also three small black holes surrounding one bright Ag trimer (with extra Ag on top). The above two types of Si trimers do not have any surface state down to 1.5 eV below the Fermi level. The remaining three Si trimers that appear grey in filled-state STM images form the third type, which has surface density of states in an energy range of 0.5–1.5 eV below the Fermi level. If one just counts the number of Si trimers, the ratio of the three types is 1:3:3. Obviously, the split of the Si trimers into three groups with different surface state structures is caused by additional adatoms that locally modify the charges on the Si trimers. One should also expect a split of the Si 2*p* core levels for the different Si trimers. This implies that the Si trimer component (S1) of the $\sqrt{3}\times\sqrt{3}$ surface will also be split into three components on the $\sqrt{21}\times\sqrt{21}$ surface with an intensity ratio of 1:3:3. According to this ratio, the small S4 component in Fig. 7 can be assigned to the first type of Si trimer (corner hole), and S1 to the second type (three black holes). The third type of Si trimer that appears grey in the STM images has a different local environment compared to the $\sqrt{3}\times\sqrt{3}$ surface. By comparing the $\sqrt{3}\times\sqrt{3}$ and $\sqrt{21}\times\sqrt{21}$ surfaces, we find that the Si 2*p* component of the third type of Si trimer shifts to a lower binding energy as indicated by the large spectral weight near the bulk component (B). We attribute the apparent increase in the intensity of the S2 and B components to an unresolved contribution from the third type of Si trimer. To conclude this part, we find that both the valence band and the Si 2*p* core-level spectra give a consistent picture, i.e., the split of the valence band and the split of the Si 2*p* component of the trimers are intrinsic characters of the $\sqrt{21}\times\sqrt{21}$-K and -Cs surfaces.

IV. CONCLUSIONS

The electronic structures of the $\sqrt{3}\times\sqrt{3}$, $\sqrt{21}\times\sqrt{21}$-K, $\sqrt{21}\times\sqrt{21}$-Cs surfaces have been investigated by valence band and core-level photoemission. Six surface state bands are found on the K- and Cs-induced $\sqrt{21}\times\sqrt{21}$ surfaces. In contrast to Ref. 12, the electronic structure of $\sqrt{21}\times\sqrt{21}$-Cs shows a clear similarity with those of the Ag- and Au-induced $\sqrt{21}\times\sqrt{21}$ phases. The formation of S_1 and S_4 can be explained by band folding of S_1 into the $\sqrt{21}\times\sqrt{21}$ SBZ. In the case of Ag/Si(111)$\sqrt{3}\times\sqrt{3}$, we show that the metallic behavior reported in the literature is related to the extra Ag. When the extra Ag is removed from the Ag/Si(111)$\sqrt{3}\times\sqrt{3}$ surface, both valence band and Si 2*p* core-level spectra exhibit intrinsically semiconducting characters. The Si 2*p* line shape of $\sqrt{21}\times\sqrt{21}$ has been discussed in terms of three different Si trimers resulting from additional adatoms on the Ag/Si(111)$\sqrt{3}\times\sqrt{3}$ surface.

ACKNOWLEDGMENTS

Support from the MAX-lab staff is gratefully acknowledged. This work was supported by the Swedish Research Council.

*Electronic address: hazha@ifm.liu.se

[1] H. M. Zhang, T. Balasubramanian, and R. I.G. Uhrberg, Phys. Rev. B **63**, 195402 (2001).
[2] H. M. Zhang, K. Sakamoto, and R. I.G. Uhrberg, Phys. Rev. B **64**, 245421 (2001).
[3] H. Aizawa, M. Tsukada, N. Sato, and S. Hasegawa, Surf. Sci. **429**, L509 (1999).
[4] Y. G. Ding, C. T. Chan, and K. M. Ho, Phys. Rev. Lett. **67**, 1454 (1991); **69**, 2452 (1992).
[5] N. Sato, T. Nagao, and S. Hasegawa, Phys. Rev. B **60**, 16083 (1999).
[6] R. I. G. Uhrberg, H. M. Zhang, T. Balasubramanian, E. Landemark, and H. W. Yeom, Phys. Rev. B **65**, 081305 (2002).
[7] X. Tong, S. Hasegawa, and S. Ino, Phys. Rev. B **55**, 1310 (1997).
[8] S. Hasegawa, K. Tsuchie, K. Toriyma, X. Tong, and T. Nagao, Appl. Surf. Sci. **162–163**, 42 (2000).
[9] X. Tong, C.-S. Jiang, and S. Hasegawa, Phys. Rev. B **57**, 9015 (1998).
[10] J. Nogami, K. J. Wang, and X. F. Lin, Surf. Sci. **306**, 81 (1994).
[11] X. Tong, Y. Sugiura, T. Nagao, T. Takami, S. Takeda, S. Ino, and S. Hasegawa, Surf. Sci. **408**, 146 (1998).
[12] C. H. Liu, I. Matsuda, H. Morikawa, H. Okino, T. Okuda, T. Kinoshita, and S. Hasegawa, Jpn. J. Appl. Phys., Part 1 **42**, 4894 (2003).
[13] J. N. Crain, K. N. Altmann, C. Bromberger, and F. J. Himpsel, Phys. Rev. B **66**, 205302 (2002).
[14] A *p*-type layer formation on the Si substrate at high temperature annealing has been studied and results will be published.
[15] T. Yokotsuka, S. Kono, S. Suzuki, and T. Sagawa, Surf. Sci. **127**, 35 (1983).
[16] L. S. O. Johansson, E. Landemark, C. J. Karlsson, and R. I. G. Uhrberg, Phys. Rev. Lett. **63**, 2092 (1989); **69**, 2451 (1992).
[17] J. M. Carpinelli and H. H. Weitering, Phys. Rev. B **53**, 12651 (1996).
[18] G. Le Lay, M. Göthelid, A. Cricenti, C. Håkansson, and P. Perfetti, Europhys. Lett. **45**, 65 (1998).
[19] X. Tong, S. Ohuchi, T. Tanikawa, A. Harasawa, T. Okuda, Y. Aoyagi, T. Kinoshita, and S. Hasegawa, Appl. Surf. Sci. **190**, 121 (2002).
[20] J. Viernow, M. Henzler, W. L. O'Brien, F. K. Men, F. M. Leibsle, D. Y. Petrovykh, J. L. Lin, and F. J. Himpsel, Phys. Rev. B **57**, 2321 (1998).
[21] F. J. Himpsel, G. Hollinger, and R. A. Pollak, Phys. Rev. B **28**, 7014 (1983).
[22] X. Tong, S. Ohuchi, N. Sato, T. Tanikawa, T. Nagao, I. Matsuda, Y. Aoyagi, and S. Hasegawa, Phys. Rev. B **64**, 205316 (2001).